



Eidgenössische Technische Hochschule Zürich  
Swiss Federal Institute of Technology Zurich

# Laminography-Adapted NAF

Semester Project

Luca Hollenstein

January 22, 2025

Advisors: Dr. Luis Barba Flores  
Department of Computer Science, ETH Zürich

---

## Abstract

This paper adapts the Neural Attenuation Field (NAF) framework for laminography and extends its application to real-world data, offering a faster and more cost-effective alternative to conventional CBCT. Our work addresses the challenges posed by laminography-specific artifacts, including adjustments to beam geometry, handling of tilted angles, and integrating masking techniques. The adapted framework demonstrates superior reconstruction quality for synthetic data, significantly reducing artifacts compared to a state-of-art iterative reconstruction algorithm. For real-world datasets, the framework is further refined to accommodate practical complexities. Although real-world results show lower contrast and some residual artifacts, the framework consistently outperforms iterative approaches and highlights its potential for practical applications. This work establishes NAF as a scalable and efficient alternative to traditional iterative algorithms and shows promise for further refinements for future work. Code available at <https://github.com/holuca>

---

# Contents

---

<b>Contents</b>	<b>ii</b>
<b>1 Introduction</b>	<b>1</b>
<b>2 Related Works</b>	<b>3</b>
2.1 NAF . . . . .	3
2.2 Laminograph . . . . .	4
2.3 Dataset . . . . .	4
2.3.1 Synthetic Data . . . . .	4
2.3.2 Real-World Data . . . . .	5
<b>3 Methodology</b>	<b>6</b>
3.1 Laminography setting . . . . .	6
3.2 Real Data and Data Formatting . . . . .	7
<b>4 Experiments</b>	<b>8</b>
4.1 Synthetic Data . . . . .	8
4.1.1 Results . . . . .	8
4.2 Real World Data . . . . .	9
4.2.1 Results with Real World Data . . . . .	11
4.2.2 Results with Mask . . . . .	12
<b>5 Conclusion</b>	<b>16</b>
<b>Bibliography</b>	<b>18</b>

## Chapter 1

---

# Introduction

---

Reconstructing medical images with high accuracy while reducing the number of projections is a significant challenge in modern medical imaging. The commonly used approach involves using X-rays to first obtain numerous projections, which are then processed to retrieve a volumetric attenuation coefficient field. Not only are the projections harmful to the human body, but this reconstruction process is computationally expensive and often impractical when only sparse views are available. Consequently, extensive research has focused on reducing the number of projections, and decreasing computational time while improving or maintaining accuracy.

One widely used method in this field is Cone Beam Computed Tomography (CBCT), which captures volumetric data from a series of projections using cone-shaped beams. One noteworthy improvement in CBCT is the Neural Attenuation Field for CBCT (NAF CBCT), a framework that leverages neural networks to achieve accurate 3D volume reconstructions from a limited number of projections [1]. We use this NAF CBCT framework and want to extend it to work for laminography settings. Laminography, a related imaging modality, is particularly useful for examining flat, thin, or layered structures, such as electronic chips or brain cells. It differs from CBCT in its use of parallel beam geometries and a tilt angle.

The goal of this project is to address some limitations of this setting by extending the principle of NAF CBCT to laminography settings. Specifically, we adapt the framework to parallel beam construction with tilt angles to facilitate high-resolution volumetric reconstructions using sparse views. The hope is that leveraging neural networks in this adapted framework can mitigate the weakness of laminography while maintaining its advantages.

Our results show significant improvement compared to the iterative algorithm. The adapted framework yielded promising reconstructions on a synthetic dataset, showcasing the potential of neural network-driven laminographic imaging. It substantially outperformed comparable iterative methods.

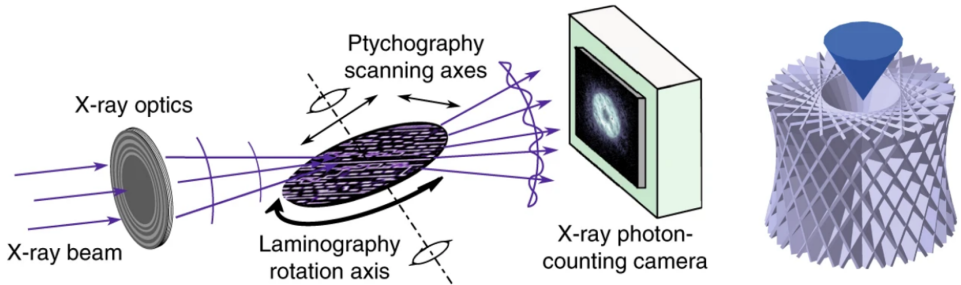


**Figure 1.1:** Left: Imaging geometry of PyXL in a laminography setting. Right: Illustration of the filling of Fourier space in laminography for  $\theta = 61^\circ$ . [2]

For real-world datasets, the adapted NAF also performed well, surpassing the current state-of-art algorithm. While the results still exhibit some noise and laminographic artifacts, further fine-tuning shows great promise. This study underscores the potential of neural approaches in advancing laminographic imaging and highlights the importance of continued refinement and exploration in this field.

## Chapter 2

---

# Related Works

---

This project builds on top of an existing framework NAF: Neural Attenuation Fields for Sparse-View CBCT Reconstruction by Zhang et al. [1], which integrates NeRF-like implicit representation for attenuation fields. Specifically, this work extends NAF by adapting it to laminographic geometry and testing its performance on real-world datasets, which involves addressing challenges unique to laminography.

## 2.1 NAF

The Neural Attenuation Fields (NAF) proposed by Zhang et al.[1], is a self-supervised method designed for sparse-view cone beam computer tomography (CBCT). It aims to reduce the number of X-ray projections required for reconstructions while maintaining the quality of the results.

NAF uses the principles of Neural Radiance Fields [3] (NeRF) by modeling attenuation as a spatially varying field. Specifically, it parameterizes the 3D attenuation coefficients as a continuous function using implicit neural representations (INR) [4]. This approach maps 3D spatial coordinates to attenuation values using a fully connected deep neural network (MLP). Unlike traditional CBCT methods, NAF operates without requiring external training datasets, relying only on the projections of the object we want to reconstruct. As intended, NAF is particularly effective in sparse-view CBCT scenarios. Synthesizing high-quality X-ray projections and learning to interpolate missing data successfully fills in gaps in undersampled datasets, producing reconstructions with reduced artifacts and high fidelity. We want to use this property for our laminography setting and hope it compensates for its problems. Furthermore, its lightweight design enables the reconstruction of high-quality CT models in significantly less time than iterative methods while maintaining state-of-the-art accuracy.

However, NAF has certain limitations. It relies on isotropic data for accurate

reconstruction, which poses challenges when applied to flat objects. Flat samples often exhibit anisotropic resolution, with high detail in the plane but poor resolution perpendicular to it. Moreover, we want to test NAF on real ptycho-tomographic data using the newly adapted NAF for laminography settings.

## 2.2 Laminograph

Laminography is similar to CBCT but is aimed at imaging flat or layered samples that are unsuitable for conventional computed tomography (CT). Unlike CT, where the object rotates fully around an axis orthogonal to the beam direction, laminography acquires projections using a specific tilt angle. A key difference between laminography and CBCT is the use of parallel beams instead of cone beams. Parallel beams are preferred because they provide uniform illumination and avoid the perspective distortions inherent to cone beams, which are less effective for flat objects. Additionally, parallel beams simplify reconstruction by avoiding the central magnification effects that cone beams introduce, making them more suitable for imaging large, flat areas.

Despite its advantages, laminography faces challenges in reconstruction due to incomplete sampling in Fourier space. The tilted axis geometry leads to undersampled or unsampled regions, often referred to as "missing wedges" [5]. This uneven sampling density results in directional artifacts or blurring in the reconstructed volume. The integration of NAF into laminography aims to address these challenges by leveraging its ability to interpolate missing data in undersampled Fourier regions. By incorporating learned patterns from similar data, NAF has the potential to fill these gaps and enhance reconstruction quality, particularly for applications requiring precise imaging of flat samples.

## 2.3 Dataset

This work evaluates the performance of the adapted Neural Attenuation Fields (NAF) framework on both synthetic and real-world datasets. The datasets include simulated integrated chip circuits and real ptychographic tomography data of brain tissue, presenting inherent noise, anisotropic properties, and complexity to test the robustness and adaptability of our adapted NAF framework.

### 2.3.1 Synthetic Data

The synthetic dataset consists of integrated circuit volumes generated from their Graphic Database System (GDS-II) photolithographic mask layout files.

These circuits have 16 nm fin field-effect transistor (FinFET) technology designed for general-purpose logic applications. The generated volumes have a resolution of  $128 \times 128 \times 128$  voxels, providing sufficient detail to evaluate reconstruction quality. The laminographic projections for these volumes were simulated using a tilt angle of 29 degrees, which is representative of realistic laminography setups. These synthetic projections serve as ground truth for evaluating our method's ability to reconstruct accurate attenuation fields and minimize artifacts under controlled conditions.

### 2.3.2 Real-World Data

To validate the framework in practical scenarios, we employed a high-resolution brain dataset from mice, obtained through ptychographic X-ray computed tomography (PyXL). This dataset was measured at the cSAXS beamline of the Swiss Light Source at the Paul Scherrer Institute, Switzerland. The brain samples were prepared using a diamond knife for polishing and trimming, followed by fine-tuning with a 30 keV gallium beam to expose histological layers of interest. MicroCT imaging was used to define these layers prior to mounting the samples on a holder for ptychographic imaging.

The dataset features a voxel size ranging from 37.5 nm to 40.0 nm, offering good detail of the brain's structure, including neurons and synapses. Each tomogram originally has a size of  $128 \times 736 \times 736$  voxels, capturing detailed histological structures in high quality. For the purposes of this work, the dataset was downsampled to  $128 \times 356 \times 356$ , balancing resolution and computational constraints.

## Chapter 3

---

# Methodology

---

The objective of this work is to adjust the NAF framework for the laminography setting and make it applicable to real-world data. Laminography is similar to tomography uses a parallel beam geometry and introduces tilt angles for the X-rays, compared to the perpendicular beam geometry in conventional tomographic settings. Additionally, this project extends NAF's applicability to real ptycho-tomographic data. Achieving this required modifications to both geometry and data handling.

### 3.1 Laminography setting

The Cone Geometry class in NAF provides several configurable parameters, allowing for straightforward adjustments to simulate parallel beam geometry. By setting the distance from source to detector (DSD) to infinity, we effectively simulate parallel beam geometry. Additional parameters, such as magnification and detector size, were fine-tuned to align with the laminography setup. The introduction of the tilt angle required modifications to the beam's origin and orientation. Specifically, the beam origin was translated upward to align with the object in the middle of the plane and an additional rotation was applied to the beam to simulate the tilt angle. Some constraints are introduced due to the changes like the tilted beam geometry no longer covering the entire object and flipping of the object orientation in some projections, requiring careful preprocessing.

Additionally, the calculations for the depth of the nearest and farthest points of the object along the beam's path were modified to accommodate the laminographic setup. To ensure the correctness of these adjustments, we tested the implementation on synthetic laminography data where the ground truth was available, validating the accuracy of the adapted NAF geometry.

Efforts to improve reconstruction quality included applying total variation (TV) regularization and addressing gaps in Fourier space inherent to laminog-

### 3.2. Real Data and Data Formatting

raphy. TV regularization enforced smoothness in the 3D domain, while Fourier domain regularization targeted spectral inconsistencies. Despite these efforts, the improvements were minimal, with no significant changes in loss metrics or visual quality observed.

## **3.2 Real Data and Data Formatting**

NAF originally generates synthetic projections using the tomographic toolbox TIGRE [6], a widely-used framework for simulating X-ray projections based on predefined CT geometries. To integrate real-world data into NAF, we reformatted our projections to fit the TIGRE-based standard. A custom script was developed to create a pickle file compatible with the laminography-adjusted NAF framework. While normalization was guided by prior knowledge from NAF’s synthetic datasets and is not strictly necessary if enough epochs are run, it ensures compatibility and improves performance during training. Moreover, the real-world dataset consisted of complex-valued projections, with critical information encoded in the phase component. Minor adjustments were made for the framework to handle such datasets, ensuring it works for both complex and real-valued inputs. Additionally, we implemented a masking strategy to exclude regions of the projections containing no useful information. This mask was generated based on prior knowledge about noisy or irrelevant regions of the projections, effectively improving reconstruction quality by focusing the loss calculation only on meaningful areas.

A significant challenge arose from the inclusion of both positive and negative values in the real-world dataset. NeRF-based models, including the hash encoder used in our implementation, originally assumed positive-only input values for encoding and mapping operations. To address this, we replaced the final activation function, switching from sigmoid to tanh or identity. Switching to the new activation functions enabled the network to output both positive and negative values. However, proper scaling of the final layer’s output was necessary to match the ground truth range. Experiments showed that using tanh as the final activation yielded better results, but further refinement of the tanh scaling and shifting approach could offer improvements. Future work will explore automatic scaling adjustments within the encoder to accommodate datasets with broader input ranges, aiming to ensure compatibility without additional preprocessing steps.

## Chapter 4

---

# Experiments

---

This section evaluates our adapted Neural Attenuation Fields (NAF) framework on both synthetic and real-world data. To assess its practical utility, we compare it against two reconstruction algorithms: a gradient-based iterative algorithm and the Filtered Back Projection (FBP) method.

The iterative algorithm minimizes reconstruction loss by repeatedly updating pixel values using gradients until convergence. While it can yield high-quality results, it is computationally expensive and struggles with undersampled or artifact-prone data like that in laminography. In contrast, FBP reconstructs volumes by filtering projections in the Fourier domain and back-projecting them, offering computational efficiency but being highly sensitive to noise and undersampling, often resulting in artifacts.

### 4.1 Synthetic Data

We utilize 360 projections taken with an angle of 29 degrees of a synthetic chip to benchmark our algorithm against the reconstruction of comparable algorithms, which have been optimized to their convergence. Although our model converges efficiently, additional computation can enhance its precision. For this evaluation, we trained the model for 2000 epochs with 256 rays, each sampling 1500 points. If memory allows we can use more rays and fewer epochs to improve on time efficiency.

#### 4.1.1 Results

Figure 4.1 presents five slices of the predicted density volume of the chip. The first row shows the ground truth, the second row depicts the iterative reconstruction, and the third row illustrates the output of our algorithm. Figure 4.2 displays the same object from a top-down perspective. The iterative reconstruction demonstrates noticeable blurring and artifacts, especially when viewed from the side (Figure 4.1). These artifacts, which are inherent

## 4.2. Real World Data

to laminography, include elongation and distortions due to the tilted beam geometry. Our model, while not entirely free of artifacts, significantly reduces these issues. In Figure 4.2, which shows the top-down view, some remaining artifacts related to the tilt angle can be observed. Nonetheless, visually, our method delivers a significant improvement over the iterative approach. This improvement is quantitatively supported by the metrics in Table 4.1. Our model consistently outperforms the iterative approach, particularly in the 3DSSIM and 3D PSNR. Additionally, our method is likely faster than the iterative reconstruction algorithm due to its efficient neural representation and parallelizable nature.

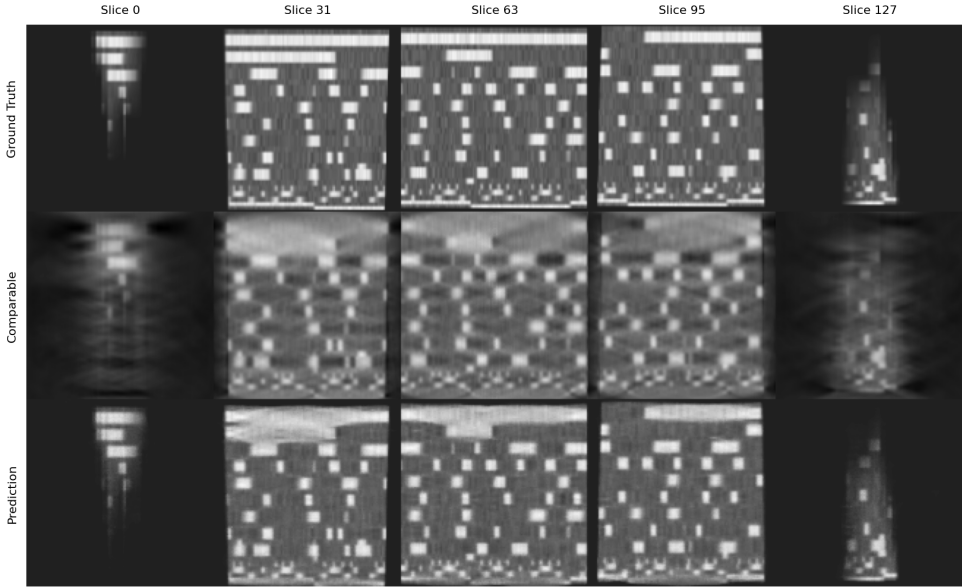


**Figure 4.1:** Visualization of the evaluation slices: Side-view. Row 1: Ground Truth, Row 2: Iterative Algorithm, Row 3: Ours

The results of the synthetic data demonstrate that our algorithm effectively minimizes artifacts and achieves higher fidelity compared to that of iterative reconstruction, solidifying its potential as a superior alternative in laminography settings.

## 4.2 Real World Data

The real-world dataset consists of 780 projections of a brain with a tilt-angle of 29 degrees, and we compare our method’s performance against the iterative reconstruction algorithm and the Filtered Back Projection Algorithm (FBP). Processing real-world data needs specific adaptations to the laminography-adapted NAF framework, including:

## 4.2. Real World Data

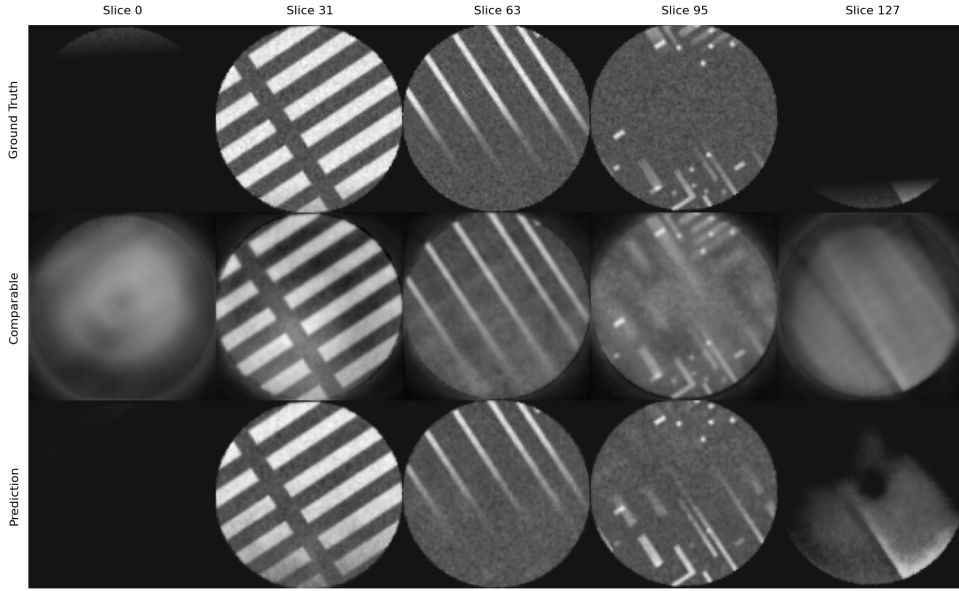


**Figure 4.2:** Visualization of the evaluation slices: Top-view. Row 1: Ground Truth, Row 2: Iterative Algorithm, Row 3: Ours

Metric	Iterative Algorithm	Ours
3D PSNR (dB)	17.18	<b>20.51</b>
3D SSIM	0.62	0.84
Average 2D PSNR (dB)	17.31	20.92
Average 2D SSIM	0.54	0.82

**Table 4.1:** Comparison of metrics between the iterative algorithm and ours. The Average 2D PSNR and Average 2D SSIM is computed from the side view which can be seen in figure 4.1.

- Setting the final activation function to tanh or the identity, to accommodate the inclusion of both positive and negative values.
- Flipping dimensions as required by the dataset format.
- Normalizing the projections to ensure numerical stability, faster convergence and interpretability during training and inference.

Real-world reconstructions for the brain require higher-resolution input images to capture fine details accurately as we aim to observe smaller details. However, memory constraints limit the image size and complexity that can be processed. As a result, fully exploring the potential of our method for

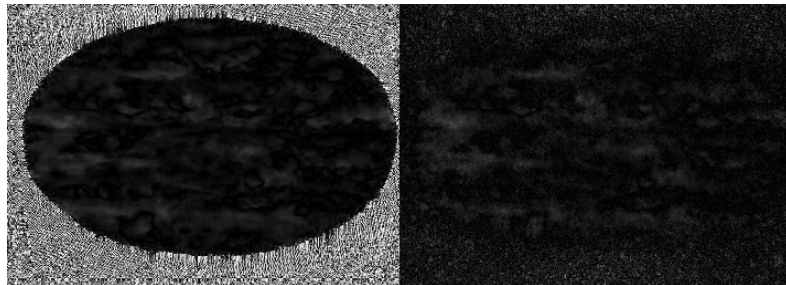
high-resolution real-world data remains challenging.

We trained the model with two configurations: no activation function in the final layer (labeled `none`) and `tanh` as the final activation function. While `tanh` generally converges faster, it requires appropriate scaling and shifting, unlike the `none` configuration, which may need more epochs for comparable results. All experiments were run for 2000 epochs with 200 rays, each sampling 2000 points.

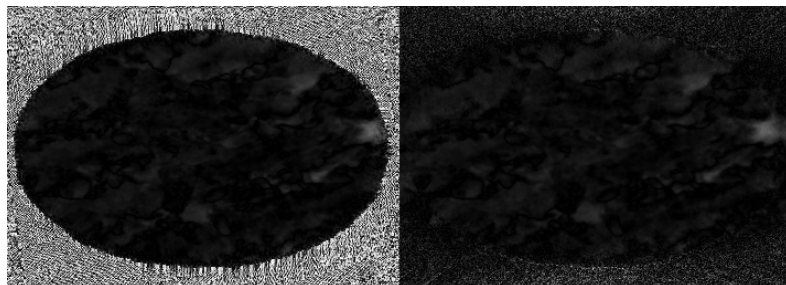
#### 4.2.1 Results with Real World Data

Figure 4.5 shows four slices of the reconstructed attenuation field. Row 1 represents the iterative algorithm’s output and row 2 the reconstruction using FBP, while rows 3 and 4 depict our model’s predictions using `none` and `tanh`, respectively. The artifacts present in the iterative reconstruction are noticeably reduced in our adapted NAF method. Using `tanh` as the final activation function yields better contrast and improved reconstructions compared to the `none` configuration, though the latter serves as a useful baseline for comparison. At this stage, the FBP still shows better reconstruction quality, as more details are depicted and our algorithm seems more blurry.

Figure 4.3 demonstrates that the reconstructed projections closely resemble the input, further validating the accuracy of our method.



**Figure 4.3:** Left: Input projection. Right: Reconstructed projection (`tanh`, no mask).



**Figure 4.4:** Left: Input projection. Right: Reconstructed projection (`tanh`, with mask).

### 4.2.2 Results with Mask

To focus the reconstruction on regions of interest, we applied masking during loss computation. This approach suppresses noisy, irrelevant regions, particularly in the outer areas, and emphasizes the brain volume at the center. Rows 5 and 6 of Figure 4.5 illustrate reconstructions using this masking approach. The application of the mask improved both interpretability and convergence speed. Note that, reconstructions with tanh as the final activation function reveal more details, closely resembling the slices of FBP, as shown in Figure 4.6. These reconstructions exhibit reduced blurriness and clearer outlines of cellular structures.

However, challenges persist, particularly with noise and low resolution, which are a problem for clearer visualization. Figure 4.7, which is a sagittal view of the volume, highlights the remaining missing cone artifacts, such as directional blurring, streaks or bands aligned with the tilt direction, and elongations. These features underscore the inherent limitations of laminographic reconstruction, even with advanced methods like masking and optimized activation functions.

## 4.2. Real World Data

---

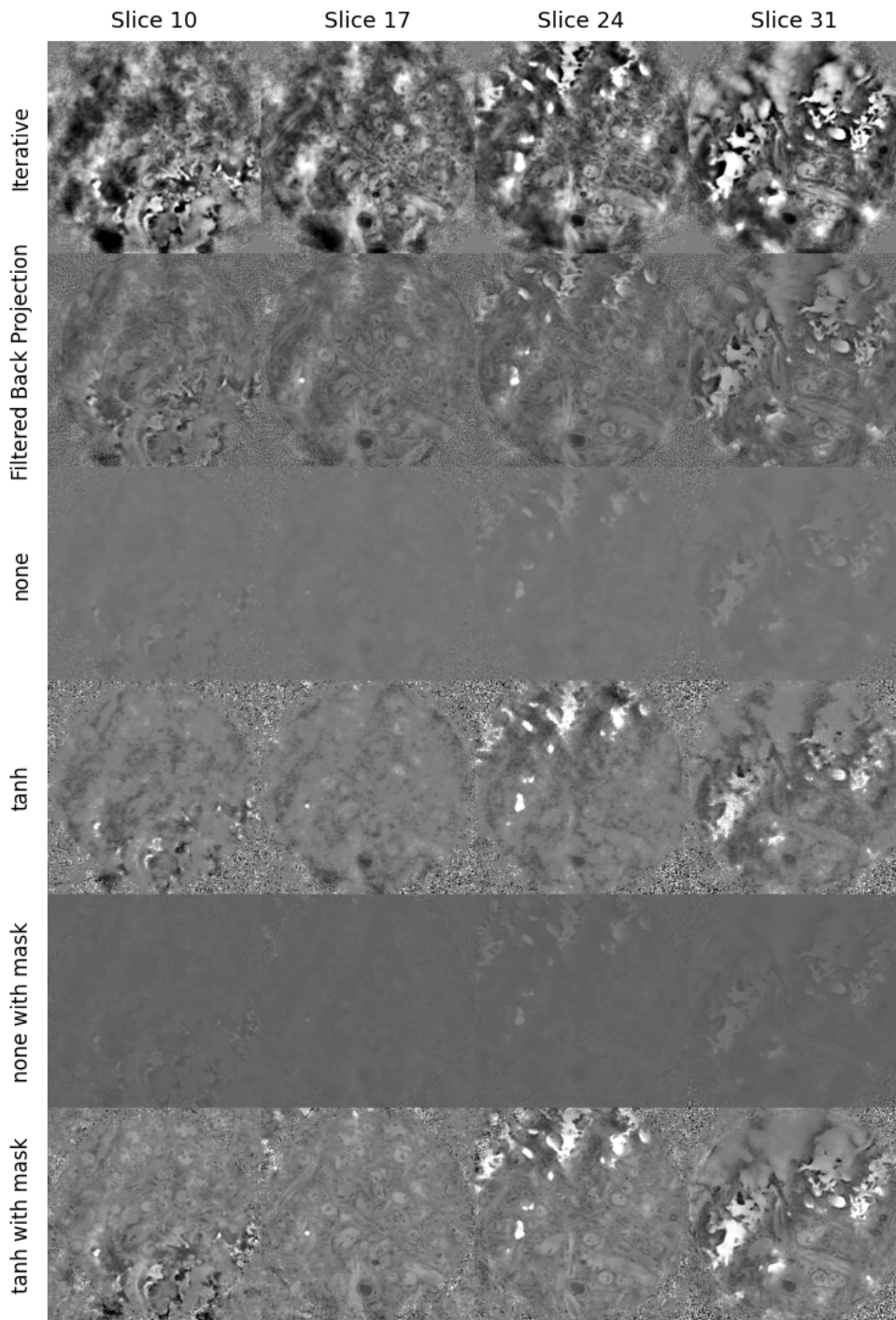


**Figure 4.5:** Four slices of the predicted attenuation field. **Row 1:** Iterative Algorithm. **Row 2:** Filtered Back Projection **Row 3:** none. **Row 4:** tanh. **Row 5:** none with mask. **Row 6:** tanh with mask.

## 4.2. Real World Data

---

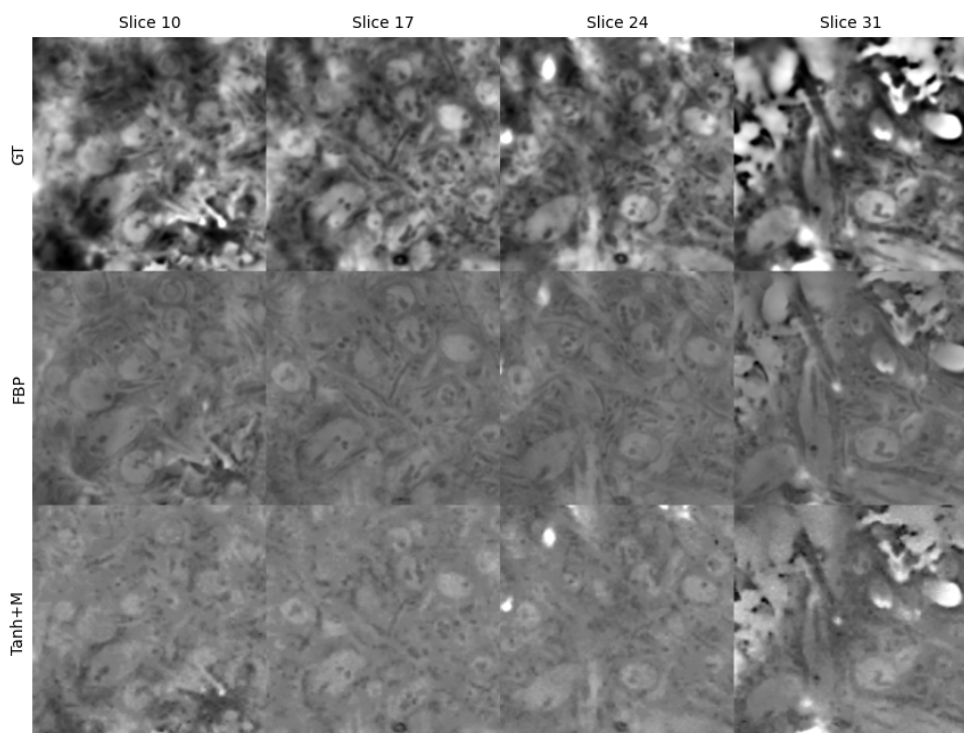


**Figure 4.6:** Zoomed in slices of the Row 1: iterative algorithm, Row 2: FBP, Row 3: Ours

## 4.2. Real World Data

---

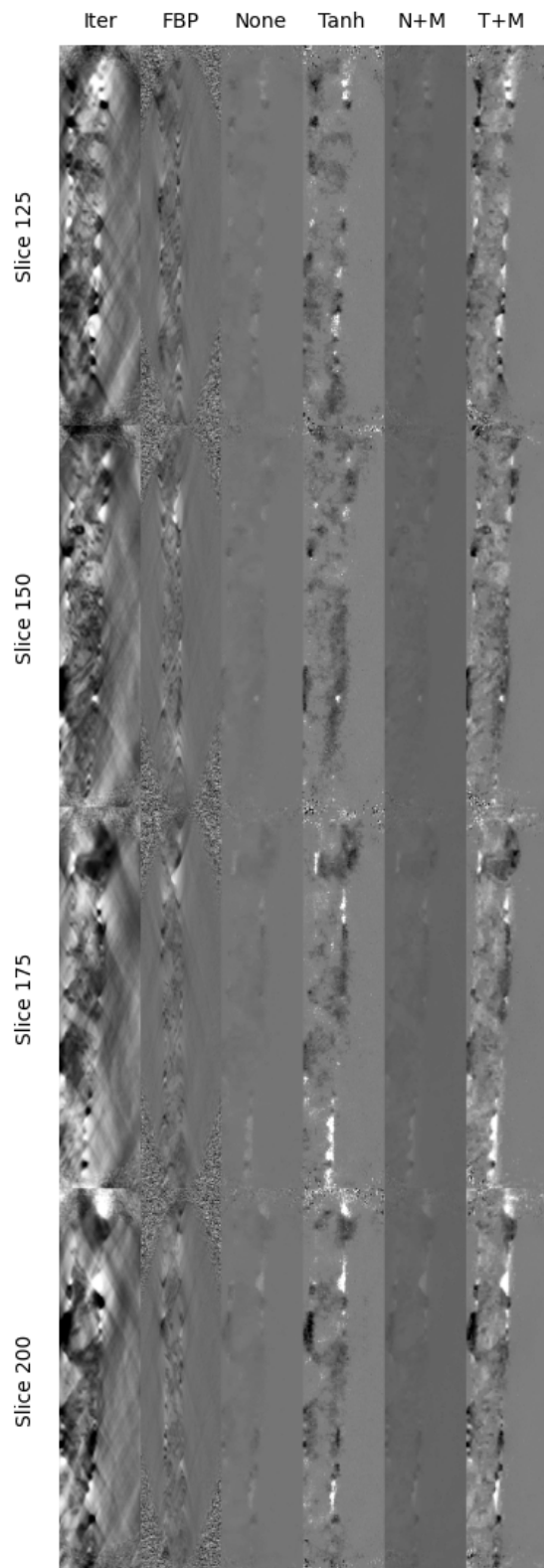


**Figure 4.7:** Sagittal View for the 6 reconstructions

## Chapter 5

---

# Conclusion

---

In this work, we successfully adapted the Neural Aggregated Fields (NAF) framework for the laminography setting and extended its application to real-world data. Laminography poses unique challenges compared to conventional tomography due to its parallel beam geometry and tilted beam configuration, both of which introduce artifacts and complicate reconstruction. Our modifications, including adjustments to the geometry, handling of tilted beams, and integration of regularization techniques, have enabled NAF to address these challenges effectively.

For synthetic data, the results demonstrate that our adapted NAF framework consistently outperforms the state-of-the-art iterative reconstruction algorithm. By leveraging the flexibility of neural representations and the efficiency of NAF, our method achieves better reconstruction quality with fewer artifacts and significantly higher accuracy. Specifically, we managed to reduce prominent laminography-specific artifacts, such as elongations and distortions, while achieving better metrics like PSNR and SSIM. The results also highlight the scalability and computational efficiency of our approach, making it a practical alternative to iterative methods.

For real-world data, our adapted framework produced meaningful reconstructions despite significant memory constraints. The results demonstrate that the reconstructed projections, particularly with masking applied, closely resemble the inputs and maintain structural coherence. While the reconstructed attenuation fields align with those of the FBP algorithm, they do not necessarily surpass it in clarity or ease of interpretation. The reconstructions remain noisy and low-resolution, highlighting the need for further refinement and the impact of limited computational resources.

Despite these achievements, some laminography artifacts remain unresolved. Certain patterns and distortions, particularly those arising from the tilted beam geometry persist in the reconstructions. These artifacts highlight areas

---

for further improvement in the framework, potentially through enhanced regularization strategies or more sophisticated neural architectures. Additionally, while our method is already faster than iterative approaches, its performance could be further optimized with greater computational resources and memory, allowing for larger network architectures and more precise sampling.

In conclusion, this work demonstrates the potential of adapting neural field-based methods like NAF for laminography and real-world applications. The ability to reduce artifacts, achieve higher fidelity, and maintain computational efficiency positions NAF as a promising tool for advancing reconstruction techniques in laminography. Future work will aim to refine the framework further, address the remaining artifacts, and enhance its applicability to broader real-world datasets.

---

## Bibliography

---

- [1] R. Zha, Y. Zhang, and H. Li, “Naf: Neural attenuation fields for sparse-view cbct reconstruction,” in *Medical Image Computing and Computer Assisted Intervention – MICCAI 2022*. Springer Nature Switzerland, 2022, pp. 442–452, ISBN: 9783031164460. doi: [10.1007/978-3-031-16446-0\\_42](https://doi.org/10.1007/978-3-031-16446-0_42). [Online]. Available: [http://dx.doi.org/10.1007/978-3-031-16446-0\\_42](http://dx.doi.org/10.1007/978-3-031-16446-0_42).
- [2] M. Holler *et al.*, “Three-dimensional imaging of integrated circuits with macro- to nanoscale zoom,” *Nature Electronics*, vol. 2, no. 10, pp. 464–470, Oct. 2019, ISSN: 2520-1131. doi: [10.1038/s41928-019-0309-z](https://doi.org/10.1038/s41928-019-0309-z). [Online]. Available: <https://doi.org/10.1038/s41928-019-0309-z>.
- [3] B. Mildenhall, P. P. Srinivasan, M. Tancik, J. T. Barron, R. Ramamoorthi, and R. Ng, *Nerf: Representing scenes as neural radiance fields for view synthesis*, 2020. arXiv: [2003.08934 \[cs.CV\]](https://arxiv.org/abs/2003.08934). [Online]. Available: <https://arxiv.org/abs/2003.08934>.
- [4] J. J. Park, P. Florence, J. Straub, R. Newcombe, and S. Lovegrove, *Deepsdf: Learning continuous signed distance functions for shape representation*, 2019. arXiv: [1901.05103 \[cs.CV\]](https://arxiv.org/abs/1901.05103). [Online]. Available: <https://arxiv.org/abs/1901.05103>.
- [5] H. Fathi and T. Leeuwen, *Source design optimization for depth image reconstruction in x-ray imaging*, Apr. 2024. doi: [10.20944/preprints202404.0960.v1](https://doi.org/10.20944/preprints202404.0960.v1).
- [6] A. Biguri, M. Dosanjh, S. Hancock, and M. Soleimani, “Tigre: A matlab-gpu toolbox for cbct image reconstruction,” *Biomedical Physics Engineering Express*, vol. 2, no. 5, p. 055 010, Sep. 2016. doi: [10.1088/2057-1976/2/5/055010](https://doi.org/10.1088/2057-1976/2/5/055010). [Online]. Available: <https://doi.org/10.1088/2057-1976/2/5/055010>.

## Declaration of originality

The signed declaration of originality is a component of every semester paper, Bachelor's thesis, Master's thesis and any other degree paper undertaken during the course of studies, including the respective electronic versions.

Lecturers may also require a declaration of originality for other written papers compiled for their courses.

---

I hereby confirm that I am the sole author of the written work here enclosed and that I have compiled it in my own words. Parts excepted are corrections of form and content by the supervisor.

**Title of work** (in block letters):

**Authored by** (in block letters):

*For papers written by groups the names of all authors are required.*

**Name(s):**

---

---

---

---

---

**First name(s):**

---

---

---

---

---

With my signature I confirm that

- I have committed none of the forms of plagiarism described in the '[Citation etiquette](#)' information sheet.
- I have documented all methods, data and processes truthfully.
- I have not manipulated any data.
- I have mentioned all persons who were significant facilitators of the work.

I am aware that the work may be screened electronically for plagiarism.

**Place, date**

**Signature(s)**

---

---

---

---

---

*For papers written by groups the names of all authors are required. Their signatures collectively guarantee the entire content of the written paper.*